

Stop searches in flavourful supersymmetry

Andreas Crivellin,^{a,d} Ulrich Haisch^{b,d} and Lewis C. Tunstall^c

^a*Paul Scherrer Institut, CH-5232 Villigen PSI, Switzerland*

^b*Rudolf Peierls Centre for Theoretical Physics, University of Oxford,
1 Keble Road, Oxford OX1 3NP, United Kingdom*

^c*Albert Einstein Center for Fundamental Physics, Institute for Theoretical Physics,
University of Bern, Sidlerstrasse 5, CH-3012 Bern, Switzerland*

^d*CERN, Theory Division, CH-1211 Geneva 23, Switzerland*

E-mail: andreas.crivellin@cern.ch, ulrich.haisch@physics.ox.ac.uk,
tunstall@itp.unibe.ch

ABSTRACT: Natural realisations of supersymmetry require light stops \tilde{t}_1 , making them a prime target of LHC searches for physics beyond the Standard Model. Depending on the kinematic region, the main search channels are $\tilde{t}_1 \rightarrow t\tilde{\chi}_1^0$, $\tilde{t}_1 \rightarrow Wb\tilde{\chi}_1^0$ and $\tilde{t}_1 \rightarrow c\tilde{\chi}_1^0$. We first examine the interplay of these decay modes with $\tilde{c}_1 \rightarrow c\tilde{\chi}_1^0$ in a model-independent fashion, revealing the existence of large regions in parameter space which are excluded for any $\tilde{t}_1 \rightarrow c\tilde{\chi}_1^0$ branching ratio. This effect is then illustrated for scenarios with stop-scharm mixing in the right-handed sector, where it has previously been observed that the stop mass limits can be significantly weakened for large mixing. Our analysis shows that once the LHC bounds from $\tilde{c}_1 \rightarrow c\tilde{\chi}_1^0$ searches are taken into account, non-zero stop-scharm mixing leads only to a modest increase in the allowed regions of parameter space, with large areas excluded for arbitrary mixing angles.

Contents

1	Introduction	1
2	Stop search combination for $m_{\tilde{t}_1} - m_{\tilde{\chi}_1^0} > m_t$	3
3	Stop search combination for $m_W + m_b < m_{\tilde{t}_1} - m_{\tilde{\chi}_1^0} < m_t$	8
4	Exclusion limits for purely right-handed up-squark mixing	11
5	Conclusions and outlook	14
A	Event generation	15

1 Introduction

A key feature of supersymmetric extensions of the Standard Model (SM) is the fact that radiative corrections to the Higgs potential can induce electroweak symmetry breaking in a technically natural fashion. Since top quarks and top squarks dominate the radiative corrections, naturalness requires their masses to be of similar magnitudes to ensure a sufficient cancellation of quadratic divergences. Apart from the gluino, Higgsinos and the left-handed bottom squark, the rest of the superpartners are less important for naturalness, and may well have masses above the reach of the LHC [1–6]. A spectrum with the above hierarchy is a typical starting point for phenomenological analyses in supersymmetry (SUSY).

Although light stops are required for naturalness, they can reintroduce fine-tuning in minimal SUSY because the Higgs is typically predicted to be light. For instance, to accommodate a Higgs mass of 125 GeV in the Minimal Supersymmetric SM (MSSM), the stop masses must be around 1 TeV, at the cost of tuning at the percent level or worse. Reconciling these two features, light stops for naturalness and heavier stops for the Higgs mass, constitutes the “little hierarchy problem”. However, in contrast to naturalness, the little hierarchy problem is model dependent and tightly bound to the MSSM. SUSY models that can generate a sufficiently heavy Higgs with improved naturalness include scenarios with non-decoupling D -terms [7] and the next-to-minimal supersymmetric SM with special parameter choices [8].

Naturalness considerations aside, there are additional reasons to expect light stops if SUSY is realised in nature. For instance, the renormalisation group evolution from a high scale with universal squark masses typically drives the masses of the third generation squarks to small values [9]. Light stops also help accommodate the observed dark matter relic density [10, 11] and are an essential ingredient in realising baryogenesis [12–14].

Experimentally, the bounds on the lightest stop mass $m_{\tilde{t}_1}$ are much weaker than the limits on the other coloured superpartners, i.e. the squarks of the first two generations and

the gluino [15, 16]. There are three main kinematic regions where different channels are used to search for stops, namely

$$\text{R1)} \quad m_{\tilde{t}_1} - m_{\tilde{\chi}_1^0} > m_t: \quad \tilde{t}_1 \rightarrow t\tilde{\chi}_1^0,$$

$$\text{R2)} \quad m_W + m_b < m_{\tilde{t}_1} - m_{\tilde{\chi}_1^0} < m_t: \quad \tilde{t}_1 \rightarrow Wb\tilde{\chi}_1^0,$$

$$\text{R3)} \quad m_c < m_{\tilde{t}_1} - m_{\tilde{\chi}_1^0} < m_W + m_b: \quad \tilde{t}_1 \rightarrow c\tilde{\chi}_1^0 \text{ and } \tilde{t}_1 \rightarrow bff'\tilde{\chi}_1^0.$$

Here $m_{\tilde{\chi}_1^0}$ denotes the mass of the lightest neutralino, constituting the lightest superpartner (LSP), while m_W , m_b and m_c are the mass of the W boson, the bottom quark and the charm quark, respectively.

In each region, the results from the ATLAS and CMS searches are interpreted in the context of simplified models, where the branching ratio for each decay mode is fixed to 100% and flavour violation is assumed to be absent. Under these assumptions, the resulting limits on $m_{\tilde{t}_1}$ in the region R1 are strong, reaching up to stop masses close to 800 GeV [17–26]. It has been observed [27–30], however, that these limits can be weakened if non-minimal sources of flavour violation are present. This occurs because flavour-violating effects enhance the decay width for $\tilde{t}_1 \rightarrow c\tilde{\chi}_1^0$, and thereby reduce the branching ratio for $\tilde{t}_1 \rightarrow t\tilde{\chi}_1^0$ from unity. On the other hand, if the decay width of $\tilde{t}_1 \rightarrow c\tilde{\chi}_1^0$ becomes large, the limits from direct \tilde{c}_1 pair production and subsequent scharm decay $\tilde{c}_1 \rightarrow c\tilde{\chi}_1^0$ [31] become relevant, which apply to $\tilde{t}_1 \rightarrow c\tilde{\chi}_1^0$ as well once the branching ratio is large. In the second region R2, the situation is similar. The limits on $m_{\tilde{t}_1}$ reach only up to around 300 GeV [17, 19, 20] and the three-body decay $\tilde{t}_1 \rightarrow Wb\tilde{\chi}_1^0$ is suppressed by phase space, so that $\tilde{t}_1 \rightarrow c\tilde{\chi}_1^0$ can compete for relatively small off-diagonal elements in the squark mass matrix [32]. Again, once stop-scharm mixing and therefore the decay width for $\tilde{t}_1 \rightarrow c\tilde{\chi}_1^0$ is sizeable, searches for charm signatures [33] can become relevant. Finally, in the third region R3, $\tilde{t}_1 \rightarrow c\tilde{\chi}_1^0$ is typically the dominant decay mode and the four-body decay $\tilde{t}_1 \rightarrow bff'\tilde{\chi}_1^0$ [19, 33] can only compete for scenarios resembling Minimal Flavour Violation (MFV) [34].

The purpose of this article is to examine the complementarity of $\tilde{c}_1 \rightarrow c\tilde{\chi}_1^0$ searches with the standard channels $\tilde{t}_1 \rightarrow Wb\tilde{\chi}_1^0$ and $\tilde{t}_1 \rightarrow c\tilde{\chi}_1^0$ in the presence of non-minimal sources of flavour violation. In Section 2, we introduce the basic ideas behind our combination procedure and apply it to set model-independent limits on $m_{\tilde{t}_1}$, $m_{\tilde{\chi}_1^0}$ and the branching ratio of $\tilde{t}_1 \rightarrow c\tilde{\chi}_1^0$ in the kinematic region R1 using ATLAS Run I data. The very same exercise is performed in Section 3 for the region R2. Focusing on flavour mixing in the right-handed up-squark sector, which is largely unconstrained by quark flavour observables, we then quantify in Section 4 the interplay between the different search strategies. As we are interested in non-MFV scenarios in this article, we use the ATLAS bounds for $\tilde{t}_1 \rightarrow c\tilde{\chi}_1^0$ directly in region R3. This allows us to provide interesting exclusions in large parts of the entire $m_{\tilde{t}_1} - m_{\tilde{\chi}_1^0}$ plane. Our conclusions and an outlook are presented in Section 5. In order to make our article self-contained, Appendix A provides details on the Monte Carlo (MC) simulations that were used to obtain the numerical results presented in our work.

2 Stop search combination for $m_{\tilde{t}_1} - m_{\tilde{\chi}_1^0} > m_t$

We begin our numerical analysis in the kinematic region R1. In this region the two-body decay $\tilde{t}_1 \rightarrow t\tilde{\chi}_1^0$ dominates unless non-minimal sources of flavour violation in the up-squark sector are present that lead to an appreciable rate for $\tilde{t}_1 \rightarrow c\tilde{\chi}_1^0$. As illustrated in Figure 1, in such cases one faces three different decay configurations: one that involves two top quarks (configuration 1), one with an intermediate top and a charm quark (configuration 2), and finally one with two charm quarks (configuration 3). Since the final state contains two LSPs in all configurations, the visible decay products will be augmented by large amounts of missing transverse momentum ($E_{T,\text{miss}}$).

In order to find combined model-independent limits on $m_{\tilde{t}_1}$, $m_{\tilde{\chi}_1^0}$ and the branching ratio $\text{Br}(\tilde{t}_1 \rightarrow c\tilde{\chi}_1^0)$ in the region R1, we employ three different ATLAS searches that are all based on around 20 fb^{-1} of $\sqrt{s} = 8 \text{ TeV}$ data. Specifically, these are

- a) 2 c -tags + $E_{T,\text{miss}}$ [31]: This ATLAS search is originally designed for the decay configuration 3 in Figure 1. In order to maximise the sensitivity of this search, three distinct signal regions (SRs) called `mct150`, `mct200` and `mct250` are defined. In all SRs, events have to have a reconstructed primary vertex consistent with the beam positions and to meet basic quality criteria. Furthermore, events are required to contain no residual electron or muon candidate and at least two jets with radius $R = 0.4$ and $p_T > 130, 100 \text{ GeV}$ and $|\eta| < 2.5$. The multijet background contribution with large $E_{T,\text{miss}}$ is suppressed by requiring a minimum azimuthal separation $|\Delta\phi(\vec{p}_{T,j_{1,2,3}}, \vec{p}_{T,\text{miss}})| > 0.4$ between any of the three leading jets and the $E_{T,\text{miss}}$ direction $\vec{p}_{T,\text{miss}}$. The third jet is exempted from this angular requirement, if it has $p_T < 50 \text{ GeV}$, $|\eta| < 2.4$ and less than half of the sum of its track p_T is associated with tracks matched to the primary vertex. The two highest- p_T jets are required to be identified as arising from a charm quark (c -tagged). The algorithm used in the ATLAS analysis achieves a c -tagging efficiency of 20% with a b -jet and light-jet rejection fraction of 8 and 200 (medium operating point) [36]. The $E_{T,\text{miss}}$ selections are $E_{T,\text{miss}} > 150 \text{ GeV}$ and $E_{T,\text{miss}} / \sum_{i=1,2} |p_{T,j_i}| > 1/3$. To further discriminate between signal and background the invariant mass of the two c -tagged jets has to satisfy $m_{c\bar{c}} > 200 \text{ GeV}$ and a selection based on the boost-corrected contranverse mass m_{CT} [35] is employed. Depending on the SR, $m_{CT} > 150 \text{ GeV}$, $m_{CT} > 200 \text{ GeV}$ or $m_{CT} > 250 \text{ GeV}$ is required.
- b) 1 lepton + 4 jets + 1 b -tag + $E_{T,\text{miss}}$ [19]: In its original form, this ATLAS search has been tailored for the decay configuration 1 in Figure 1 with one top quark decaying hadronically and the other one leptonically. It implements four SRs that target different regions in the $m_{\tilde{t}_1} - m_{\tilde{\chi}_1^0}$ plane and implement different analysis strategies. In our case it turns out that only the SRs called `tN_diag` and `tN_med` are relevant in the combination. The following preselection criteria are common to the two SRs. Events are required to have a reconstructed primary vertex, $E_{T,\text{miss}} > 100 \text{ GeV}$, exactly one isolated lepton with $p_T > 25 \text{ GeV}$ and at least four $R = 0.4$ jets with $p_T > 25 \text{ GeV}$. Events that do not pass certain data quality requirements are re-

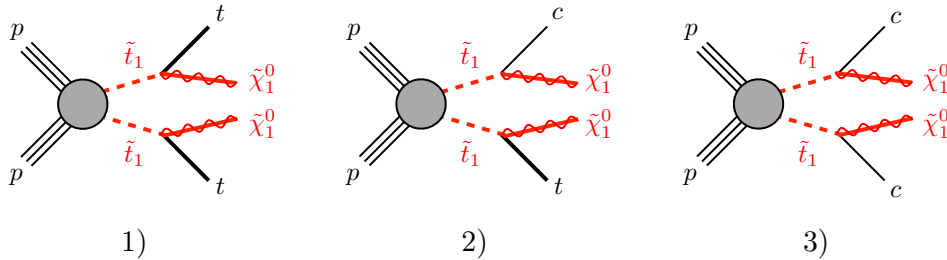


Figure 1. The three different decay configurations relevant for the combination of different stop channels in the kinematic region R1.

jected. In the SR `tN.diag`, the cuts on the three hardest jets are $p_T > 60, 60, 40$ GeV and $|\eta| < 2.5$. The two leading jets have to satisfy $|\Delta\phi(\vec{p}_{T,j_{1,2}}, \vec{p}_{T,\text{miss}})| > 0.8$ and at least one jet has to be identified as a bottom-quark jet (b -tagged), assuming an average tagging efficiency of 70% [37, 38]. In addition, we require in our analysis $E_{T,\text{miss}} > 150$ GeV, $E_{T,\text{miss}}/\sqrt{H_T} > 5$ GeV $^{1/2}$, $m_T > 140$ GeV, $m_{\text{had-top}} \in [130, 205]$ GeV and impose a veto on loose τ leptons. Here H_T is defined as the scalar p_T of the four hardest jets in the event, m_T denotes the transverse mass constructed from the lepton transverse momentum and $\vec{p}_{T,\text{miss}}$, while $m_{\text{had-top}}$ represents the hadronic top mass. The selection requirements in `tN.med` that differ from that of `tN.diag` are $p_T > 80, 60, 40$ GeV for the three leading jets, $|\Delta\phi(\vec{p}_{T,j_2}, \vec{p}_{T,\text{miss}})| > 0.8$, $E_{T,\text{miss}} > 200$ GeV and $m_{\text{had-top}} \in [130, 195]$ GeV. A cut on $E_{T,\text{miss}}/\sqrt{H_T}$ and a τ -veto is not imposed, but $H_{T,\text{miss}}^{\text{sig}} > 12.5$ and $am_{T2} > 170$ GeV is required. Here $H_{T,\text{miss}}^{\text{sig}}$ is an object-based missing transverse momentum that is normalised by the per-event resolution of the jets [19] and am_{T2} is an asymmetric variant of the generalised transverse mass [39–42].

- c) 6 jets+2 b -tags+ $E_{T,\text{miss}}$ [18]: This ATLAS search aims to provide the best sensitivity for the decay configuration 1 in Figure 1 with both top quarks decaying hadronically. In our analysis, we consider only the SR A1 and the SR A2 out of the possible nine SRs. All events that pass certain quality requirements and do not contain a reconstructed electron or muon with $p_T > 10$ GeV are subjected to the following common selection criteria. They have to have at least six $R = 0.4$ jets with $p_T > 80, 80, 35, 35, 35, 35$ GeV and $|\eta| < 2.8$, and out of these jets, two or more have to be b -tagged (70% efficiency). The number of events with mismeasured $E_{T,\text{miss}}$ is reduced by requiring $|\Delta\phi(\vec{p}_{T,j_{1,2,3}}, \vec{p}_{T,\text{miss}})| > \pi/5$ and $|\Delta\phi(\vec{p}_{T,\text{miss}}, \vec{p}_{T,\text{miss}}^{\text{track}})| < \pi/3$, where $\vec{p}_{T,\text{miss}}^{\text{track}}$ denotes the missing transverse momentum direction determined from the calorimeter system. To further sculpt the signal, the transverse mass calculated from the b -tagged jet closest in the azimuthal angle ϕ to $\vec{p}_{T,\text{miss}}$ has to satisfy $m_T^{b,\text{min}} > 175$ GeV, the mass cuts $m_{bjj}^0 < 225$ GeV and $m_{bjj}^1 < 250$ GeV on the first and second top candidate [18] are imposed and loose τ leptons are vetoed. The SRs A1 and A2 only differ in the imposed $E_{T,\text{miss}}$ selection. In the former case, events with $E_{T,\text{miss}} > 150$ GeV suffice, while in the latter case the stronger requirement $E_{T,\text{miss}} > 250$ GeV is imposed.

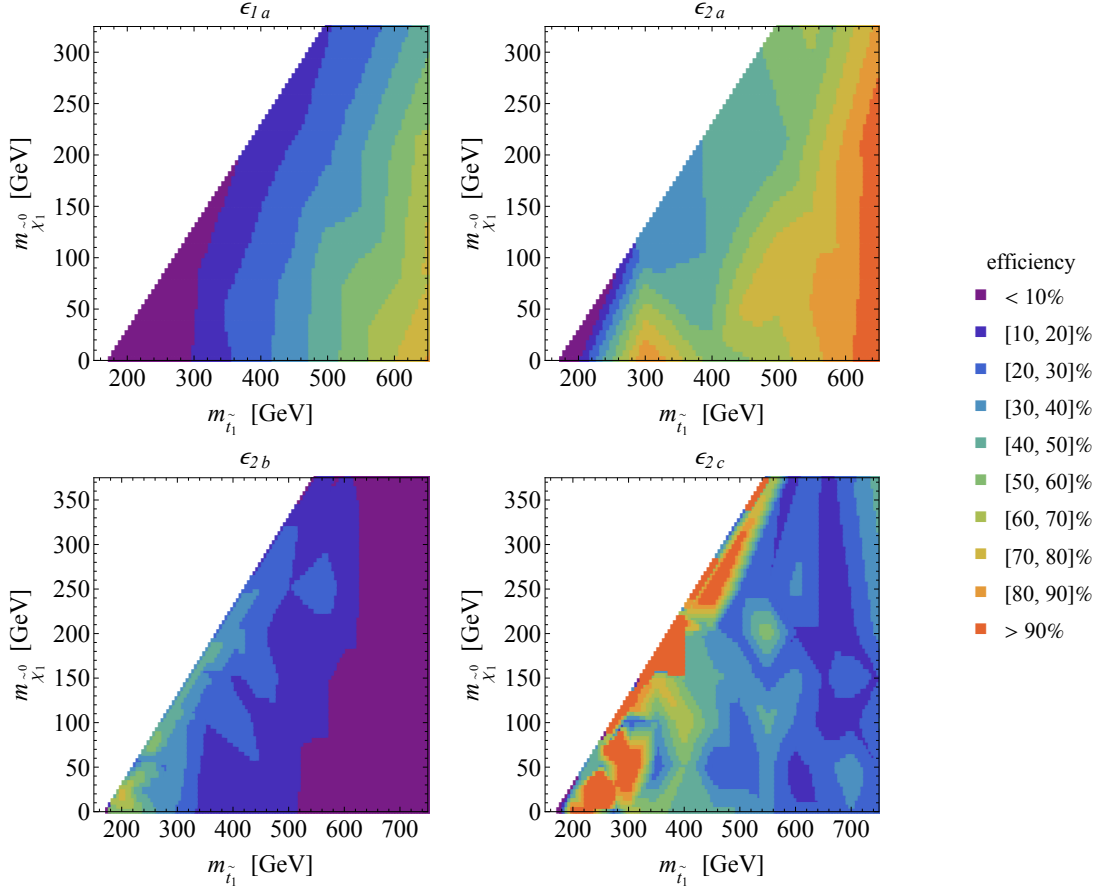


Figure 2. Efficiency maps relevant for the combination of different stop channels in the kinematic region R1. Only the non-trivial efficiencies ϵ_{1a} (upper left panel), ϵ_{2a} (upper right panel), ϵ_{2b} (lower left panel) and ϵ_{2c} (lower right panel) are shown.

To combine the searches a , b and c , we work in the narrow-width approximation and assume that only the decay modes $\tilde{t}_1 \rightarrow t\tilde{\chi}_1^0$ and $\tilde{t}_1 \rightarrow c\tilde{\chi}_1^0$ are relevant, so that $\text{Br}(\tilde{t}_1 \rightarrow t\tilde{\chi}_1^0) = 1 - \text{Br}(\tilde{t}_1 \rightarrow c\tilde{\chi}_1^0)$. Both assumptions are satisfied in the kinematic region R1. Using the shorthand notations $\text{Br} = \text{Br}(\tilde{t}_1 \rightarrow c\tilde{\chi}_1^0)$ and $\sigma_{\tilde{t}_1\tilde{t}_1^*} = \sigma(pp \rightarrow \tilde{t}_1\tilde{t}_1^*)$, the fiducial cross sections $(\sigma_{\text{fid}})_s$ corresponding to the three different ATLAS searches can then be written in the following way

$$\begin{aligned}
 (\sigma_{\text{fid}})_a &= \left\{ (1 - \text{Br})^2 \epsilon_{1a} + 2\text{Br}(1 - \text{Br}) \epsilon_{2a} + \text{Br}^2 \right\} \sigma_{\tilde{t}_1\tilde{t}_1^*}, \\
 (\sigma_{\text{fid}})_b &= \left\{ (1 - \text{Br})^2 + 2\text{Br}(1 - \text{Br}) \epsilon_{2b} + \text{Br}^2 \epsilon_{3b} \right\} \sigma_{\tilde{t}_1\tilde{t}_1^*}, \\
 (\sigma_{\text{fid}})_c &= \left\{ (1 - \text{Br})^2 + 2\text{Br}(1 - \text{Br}) \epsilon_{2c} + \text{Br}^2 \epsilon_{3c} \right\} \sigma_{\tilde{t}_1\tilde{t}_1^*}.
 \end{aligned} \tag{2.1}$$

Here ϵ_{ts} denotes the efficiency with which the decay configuration $t = 1, 2, 3$ (see Figure 1) is detected by the search $s = a, b, c$.

The efficiency maps relevant for the combination of the different stop channels in the

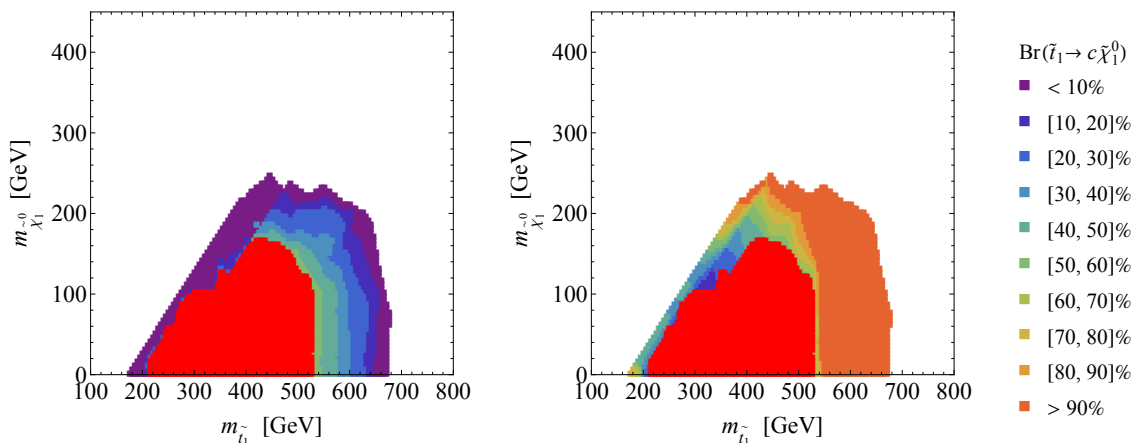


Figure 3. Lower (left panel) and upper (right panel) model-independent limit on $\text{Br}(\tilde{t}_1 \rightarrow c\tilde{\chi}_1^0)$ in the part of the $m_{\tilde{t}_1} - m_{\tilde{\chi}_1^0}$ plane corresponding to the kinematic region R1. The regions coloured red are excluded at 95% CL for any value of the $\tilde{t}_1 \rightarrow c\tilde{\chi}_1^0$ branching ratio.

region R1 are displayed in the four panels of Figure 2. They have been obtained by means of the MC simulations described in Appendix A. From the plots it is evident that the efficiencies ϵ_{ts} are not flat, but depend rather sensitively on $m_{\tilde{t}_1}$ and $m_{\tilde{\chi}_1^0}$. This behaviour is expected because changing the mass of the lightest stop and the LSP will modify the kinematic distributions of the final-state particles, which in turn leads to different signal acceptances in the various SRs. In fact, a qualitative understanding of the obtained efficiencies is possible by studying the cutflow of the analysis *a*, *b* and *c* for the different signal configurations 1, 2 and 3. We start by discussing the efficiencies ϵ_{1a} and ϵ_{2a} shown in the upper left and upper right panel of Figure 2, respectively. The first observation is that in most parts of the $m_{\tilde{t}_1} - m_{\tilde{\chi}_1^0}$ plane, the efficiency ϵ_{1a} is smaller than ϵ_{2a} . This is readily understood by recalling from Figure 1 that configuration 1 (2) leads to a final state with two bottom quarks (one bottom quark). In the former case, two *b* quarks have to be misidentified as *c*-jets in order to produce an event in the SRs of search *a*, while in the latter case one mis-tag is sufficient. Another feature that is evident from the plots is that the efficiencies ϵ_{1a} and ϵ_{2a} both decrease if one approaches the kinematic boundary of region R1. This is due to the fact that the decay chain $\tilde{t}_1 \rightarrow t\tilde{\chi}_1^0 \rightarrow W^+b\chi_1^0$ and its conjugate will not give rise to significant $E_{T,\text{miss}}$ if the mass difference $m_{\tilde{t}_1} - m_{\tilde{\chi}_1^0}$ is close to m_t , and as a result the corresponding event is less likely to pass the $E_{T,\text{miss}}$ requirements that are imposed in the scalar charm search *a*.

Simple qualitative explanations of the efficiency maps ϵ_{2b} and ϵ_{2c} presented in the lower left and lower right panel of Figure 2 can also be given. In the case of ϵ_{2b} , the requirement to have an isolated lepton strongly suppresses the acceptance for final states arising from the configuration 2, which involves both a $\tilde{t}_1 \rightarrow t\tilde{\chi}_1^0 \rightarrow W^+b\chi_1^0$ and a $\tilde{t}_1^* \rightarrow \bar{c}\tilde{\chi}_1^0$ decay or the combination of charge-conjugated processes. For these decays, the fact that a lepton with $p_T > 25$ GeV can only arise from a leptonic decay of a *W* boson also explains the finding that $\epsilon_{3b} \simeq 0$ in the whole kinematic region R1. That ϵ_{2b} increases when approaching the kinematic boundary $m_{\tilde{t}_1} - m_{\tilde{\chi}_1^0} = m_t$ has to do with the fact that

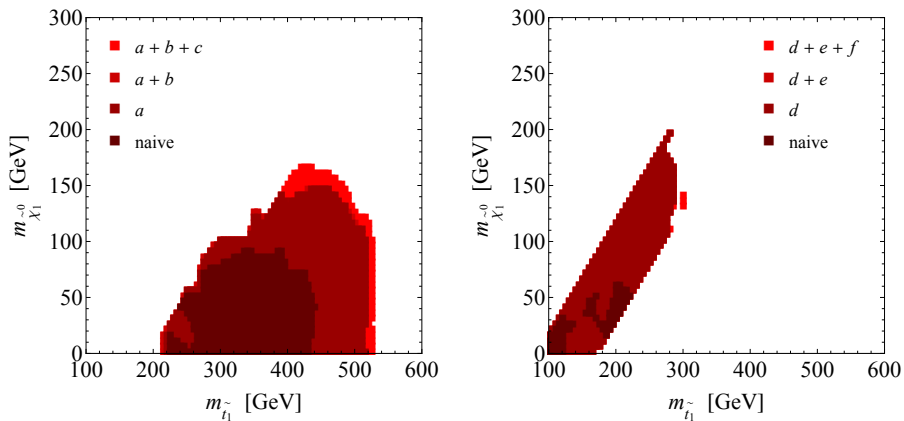


Figure 4. Comparison of the impact of the different searches strategies on the 95% CL exclusion regions in the $m_{\tilde{t}_1} - m_{\tilde{\chi}_1^0}$ plane. The left (right) panel displays the results of a naive combination and a successive inclusion of the searches a , b and c (d , e and f).

this efficiency is defined relative to the acceptance corresponding to a signal from the configuration 1 in the search b (see (2.1)). The latter acceptance is however suppressed close to the kinematic boundary because there is only little $E_{T,\text{miss}}$ available. Similar arguments hold for ϵ_{2c} . In this case the requirement that events have to contain two b -tags plays the role that the single-lepton tag played before. In fact, events resulting from configuration 2 can end up in the SR, if the final-state charm quark is erroneously b -tagged. The corresponding probability is non-negligible and taking into account that the relative acceptance for detecting the configuration 2 in the search c again increases for decreasing mass splitting $m_{\tilde{t}_1} - m_{\tilde{\chi}_1^0}$, one obtains numerically $\epsilon_{2c} \simeq 1$ for points with $m_{\tilde{t}_1} - m_{\tilde{\chi}_1^0}$ not too far from m_t . Since the probability to mistake two charm quarks for two b -jets is essentially zero, we furthermore find that $\epsilon_{3c} \simeq 0$ for all points of interest in the $m_{\tilde{t}_1} - m_{\tilde{\chi}_1^0}$ plane.

With the efficiency maps at hand, one can then use (2.1) and combine the individual searches to obtain model-independent exclusion limits on $\text{Br}(\tilde{t}_1 \rightarrow c\tilde{\chi}_1^0)$. The outcome of such an exercise is shown in Figure 3. The red region in both panels is excluded at 95% confidence level (CL) for any value of the $\tilde{t}_1 \rightarrow c\tilde{\chi}_1^0$ branching ratio. We observe that depending on the LSP (stop) mass, values of $m_{\tilde{t}_1}$ up to 530 GeV ($m_{\tilde{\chi}_1^0}$ up to 160 GeV) are ruled out by our combination of ATLAS Run I data. Outside the excluded region our procedure can be used to set lower and upper model-independent limits on $\text{Br}(\tilde{t}_1 \rightarrow c\tilde{\chi}_1^0)$ as indicated by the coloured contours in the left and right panel of the figure. This information will be used in Section 4 to put bounds in the $m_{\tilde{t}_1} - m_{\tilde{\chi}_1^0}$ plane for the case of the MSSM with a bino-like LSP and purely right-handed stop-scharm mixing.

It is also interesting to quantify the impact that each individual search has in the combination that leads to the final 95% CL exclusion limit. For the kinematic region R1, we illustrate the power of the different searches in the left panel of Figure 4. The naive combination corresponds to the choice $\epsilon_{ts} = 0$ in (2.1) and is indicated by the dark red contour in the figure. We see that a successive inclusion of the searches a , b and c enlarges the excluded area in the $m_{\tilde{t}_1} - m_{\tilde{\chi}_1^0}$ plane considerably. In fact, it is evident from the three

additional red contours that the inclusion of search *a* has the most pronounced effect in the combination, while adding searches *b* and *c* to the mix leads to either no or only a minor improvement of the exclusion limits in the $m_{\tilde{t}_1} - m_{\tilde{\chi}_1^0}$ plane. This feature nicely illustrates one of the main findings of our work, i.e. the observation that the recent ATLAS search for $\tilde{c}_1 \rightarrow c\tilde{\chi}_1^0$ [31] can be recast as a search for $\tilde{t}_1 \rightarrow c\tilde{\chi}_1^0$, and that this procedure can be used to set stringent bounds on $m_{\tilde{t}_1}$ and $m_{\tilde{\chi}_1^0}$ in models with non-minimal flavour mixing in the up-quark sector.

3 Stop search combination for $m_W + m_b < m_{\tilde{t}_1} - m_{\tilde{\chi}_1^0} < m_t$

We now turn our attention to the kinematic region R2. If stop-scharm mixing is present, both the two-body decay $\tilde{t}_1 \rightarrow c\tilde{\chi}_1^0$ and the three-body decay $\tilde{t}_1 \rightarrow Wb\tilde{\chi}_1^0$ can be phenomenologically relevant. As a result, the final states emerging from two stop decays can contain either two charm quarks (configuration 3), two bottom quarks (configuration 4) or one charm quark and one bottom quark (configuration 5). The additional decay configurations with bottom quarks are depicted in Figure 5. As indicated by the small grey blobs in this figure, the $\tilde{t}_1 \rightarrow Wb\tilde{\chi}_1^0$ transitions proceeds through an effective four-point vertex which involves the exchange of off-shell particles. In our analysis, we include for simplicity only top-quark exchange, but neglect chargino and sbottom contributions, assuming that these states are sufficiently heavy and decoupled from the spectrum.

In the kinematic region R2, we constrain the $m_{\tilde{t}_1} - m_{\tilde{\chi}_1^0}$ parameter space by again combining three different ATLAS analyses. They are all based on 20.3 fb^{-1} of total integrated luminosity collected at 8 TeV centre-of-mass energy, and implement the following search strategies:

- d) 4 jets + *c*-tags + $E_{T,\text{miss}}$ [33]: Originally, this ATLAS search has been designed to gain sensitivity to the decay configuration 3 in Figure 1. In our analysis, we consider the *c*-tagged selections C1 and C2. The events have to meet basic quality criteria and are vetoed if they contain isolated muons or isolated electrons with $p_T > 10 \text{ GeV}$. As a further preselection $E_{T,\text{miss}} > 150 \text{ GeV}$ and least one $R = 0.4$ jet with $p_T > 150 \text{ GeV}$ and $|\eta| < 2.5$ in the final state is required. To be contained in the SRs, the events are required to have at least four jets with $p_T > 30 \text{ GeV}$, $|\eta| < 2.5$ and $|\Delta\phi(\vec{p}_{T,j}, \vec{p}_{T,\text{miss}})| > 0.4$. A *b*-jet veto (2.5 rejection factor) is applied to the selected jets by using a loose *c*-tag requirement (95% efficiency) [36]. In addition, at least one of the three subleading jets has to pass the medium *c*-tag criteria mentioned earlier in the description of search *a*. The leading jet is then required to have $p_T > 290 \text{ GeV}$ and the two SRs C1 and C2 are defined with $E_{T,\text{miss}} > 250 \text{ GeV}$ and $E_{T,\text{miss}} > 350 \text{ GeV}$, respectively.
- e) 2 leptons + jets + $E_{T,\text{miss}}$ [17]: This ATLAS search targets the decay configuration 4 in Figure 5 with both *W* bosons decaying leptonically. Our analysis includes the SR L90 and L100 of this search. After passing certain quality requirements, events are preselected if they have exactly two oppositely charged leptons (muons, electrons or one charged lepton of each flavour). At least one

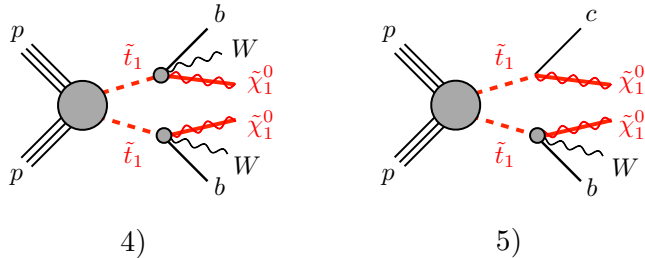


Figure 5. The two additional decay configurations that are relevant for the combination of different stop searches in the kinematic region R2.

of these leptons must have $p_T > 25$ GeV and the invariant mass of the lepton pair has to satisfy $m_{ll} > 20$ GeV. After applying these preselections, events with $m_{ll} \in [71, 111]$ GeV, $|\Delta\phi(\vec{p}_{T,j}, \vec{p}_{T,\text{miss}})| > 1$, where j denotes the jet closest to the $E_{T,\text{miss}}$ direction, and $|\Delta\phi(\vec{p}_{T,lb}, \vec{p}_{T,\text{miss}})| < 1.5$ with $\vec{p}_{T,lb} = \vec{p}_{T,l_1} + \vec{p}_{T,l_2} + \vec{p}_{T,\text{miss}}$ are rejected. The SR L90 requires $m_{T2} > 90$ GeV but has no jet requirement, while L100 has a tight jet selection with at least two $R = 0.4$ jets with $p_T > 100, 50$ GeV and $|\eta| < 2.5$. Furthermore, the cut $m_{T2} > 100$ GeV on the lepton-based stransverse mass [43, 44] is set in L100.

- f) 1 lepton + 3 jets + b -veto + $E_{T,\text{miss}}$ [19]: At the outset, this ATLAS search is intended for the decay configuration 4 in Figure 5 with one leptonic and one hadronic W -boson decay. In our combination we use the `bcC.diag` SR of this analysis, which requires one central lepton with $p_T > 25$ GeV and $|\eta| < 1.2$ as well as at least three $R = 0.4$ jets with $p_T > 80, 40, 30$ GeV and $|\eta| < 2.5$. Out of the three jets, none are allowed to be b -tagged (70% efficiency) and the two hardest jets have to satisfy $|\Delta\phi(\vec{p}_{T,j_{1,2}}, \vec{p}_{T,\text{miss}})| > 2.0, 0.8$. The other cuts in our analysis are $E_{T,\text{miss}} > 140$ GeV, $E_{T,\text{miss}}/\sqrt{H_T} > 5$ GeV $^{1/2}$, $m_T > 120$ GeV and $\Delta R(\vec{p}_{T,l}, \vec{p}_{T,j_1}) \in [0.8, 2.4]$. The angular separation in the η - ϕ plane is defined as $\Delta R = \sqrt{(\Delta\eta)^2 + (\Delta\phi)^2}$.

Under the assumption that only the decay modes $\tilde{t}_1 \rightarrow Wb\tilde{\chi}_1^0$ and $\tilde{t}_1 \rightarrow c\tilde{\chi}_1^0$ are relevant in region R2, the searches d , e and f can then be combined by using formulas analogous to those presented in (2.1). The corresponding efficiency maps are depicted in Figure 6. In the upper left and right panel we show the efficiencies for detecting final states with two bottom quarks (configuration 4) or one bottom and one charm quark (configuration 5) by means of the search d . As expected the efficiency ϵ_{4d} is typically smaller than ϵ_{5d} , because the search d involves a c -tagged selection. Another noticeable feature of the latter efficiencies is that they are enhanced close to the kinematic boundary $m_W + m_b = m_{\tilde{t}_1} - m_{\tilde{\chi}_1^0}$ for relatively light stops with $m_{\tilde{t}_1} \lesssim 250$ GeV. This is related to the fact that, compared to $\tilde{t}_1 \rightarrow c\tilde{\chi}_1^0$, the decay $\tilde{t}_1 \rightarrow Wb\tilde{\chi}_1^0$ produces a harder $E_{T,\text{miss}}$ spectrum for masses in this region of the $m_{\tilde{t}_1} - m_{\tilde{\chi}_1^0}$ plane. As a result, events resulting from configuration 4 or 5 more easily pass the $E_{T,\text{miss}}$ requirement of search d than final states arising from configuration 3.

In the lower left panel of Figure 6, we find that the efficiency $\epsilon_{5e} \simeq 0$ in the entire R2 region, as a result of the requirement of search e to have two charged leptons in each event. The very same requirement also leads to $\epsilon_{3e} \simeq 0$. The efficiency map for ϵ_{5f} is shown

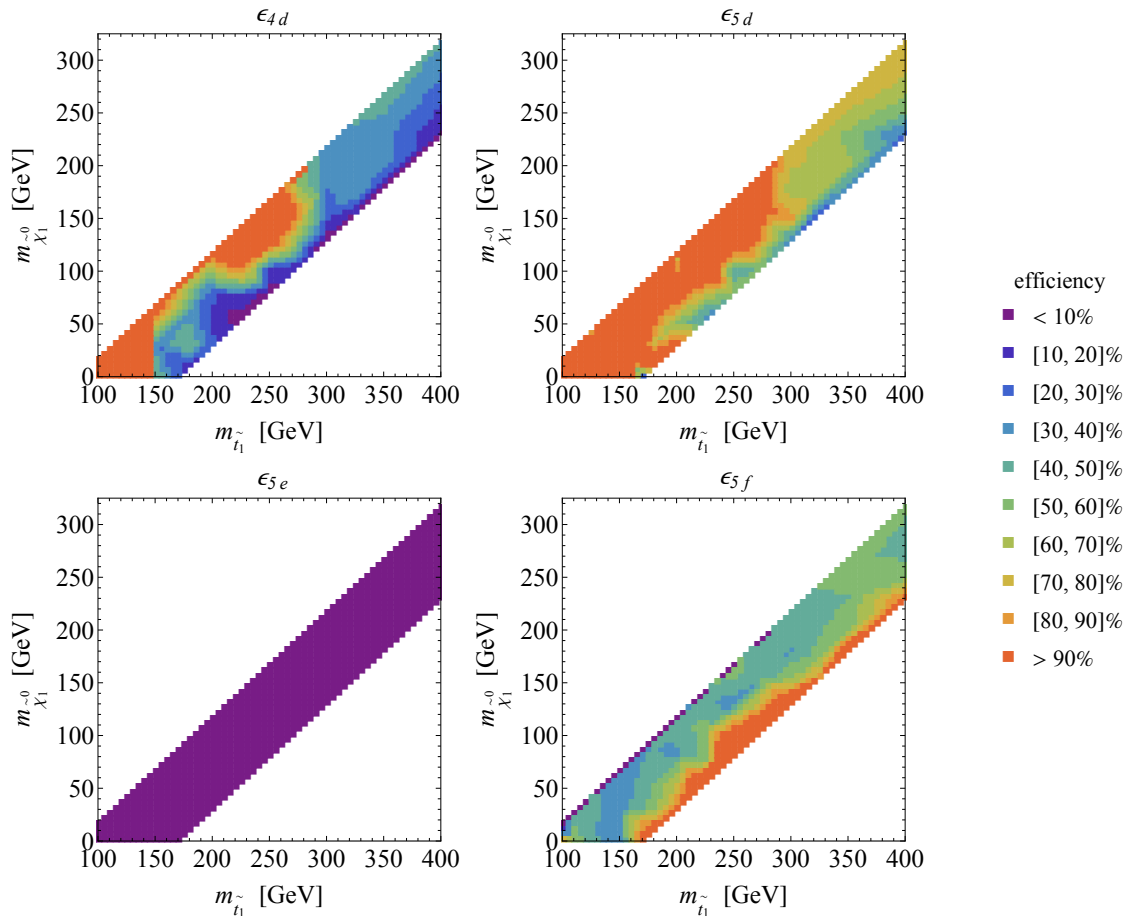


Figure 6. The efficiencies ϵ_{4d} (upper left panel), ϵ_{5d} (upper right panel), ϵ_{5e} (lower left panel) and ϵ_{5f} (lower right panel) relevant for the combination of different stop channels in region R2.

in the lower right panel of the latter figure. One observes that ϵ_{5f} grows towards masses satisfying $m_{\tilde{t}_1} - m_{\tilde{\chi}_1^0} = m_t$. This feature originates mostly from the fact that for $m_{\tilde{t}_1}$ and $m_{\tilde{\chi}_1^0}$ values close to the boundary between the regions R1 and R2, the leading jet arising from the configuration f is on average harder compared to situations where the masses are close to $m_W + m_b = m_{\tilde{t}_1} - m_{\tilde{\chi}_1^0}$. As a result of the central lepton requirement, we also find that $\epsilon_{3f} \simeq 0$ in the full R2 part of the $m_{\tilde{t}_1} - m_{\tilde{\chi}_1^0}$ plane.

In Figure 7, we show the results of our combination procedure in the case of the kinematic region R2. The parameter space that is excluded at 95% CL for any value of the $\tilde{t}_1 \rightarrow c\tilde{\chi}_1^0$ branching ratio is shaded red in both panels, while the coloured contours indicate the model-independent limits on $\text{Br}(\tilde{t}_1 \rightarrow c\tilde{\chi}_1^0)$. We see that $m_{\tilde{t}_1}$ values up to around 300 GeV are ruled out by the combined ATLAS Run I data for essentially all LSP masses $m_{\tilde{\chi}_1^0}$ satisfying $m_W + m_b < m_{\tilde{t}_1} - m_{\tilde{\chi}_1^0} < m_t$. The obtained model-independent bounds on the $\tilde{t}_1 \rightarrow c\tilde{\chi}_1^0$ branching ratio will be used in the next section to set limits in the $m_{\tilde{t}_1} - m_{\tilde{\chi}_1^0}$ plane for MSSM scenarios with a bino-like LSP and purely right-handed stop-scharm mixing.

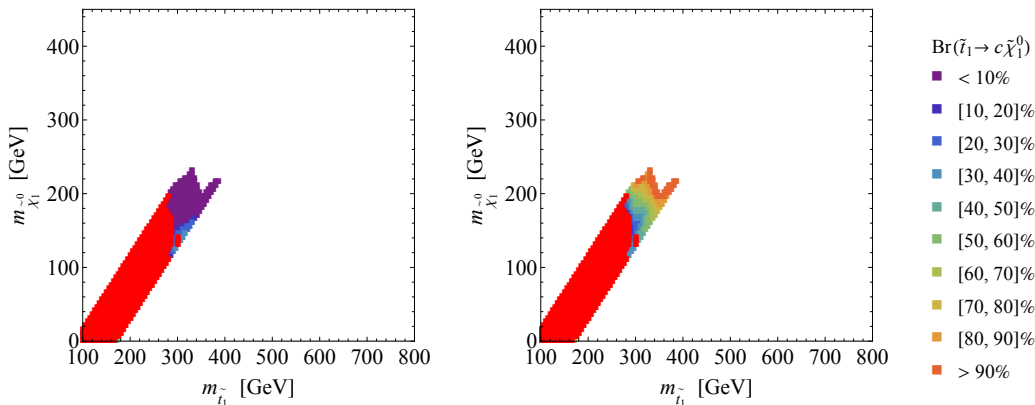


Figure 7. Model-independent lower (left panel) and upper (right panel) limits on $\text{Br}(\tilde{t}_1 \rightarrow c\tilde{\chi}_1^0)$ corresponding to $m_{\tilde{t}_1}$ and $m_{\tilde{\chi}_1^0}$ values in the kinematic region R2. The regions that are excluded at 95% CL for any value of the $\tilde{t}_1 \rightarrow c\tilde{\chi}_1^0$ branching ratio are coloured red.

As in Section 2, we finally discuss the weight that each search has in our combination. The right panel of Figure 4 shows the 95% CL exclusion contours in the kinematic region R2 that are obtained from a naive combination as well as from a successive inclusion of the searches d , e and f . From the figure it is clear that the search d has by far the strongest effect, and that adding the searches e and f does not significantly improve the exclusion in the $m_{\tilde{t}_1} - m_{\tilde{\chi}_1^0}$ plane. This again shows that c -tagged SUSY searches, like for instance the ATLAS analysis [33], can also be used to set stringent constraints on $m_{\tilde{t}_1}$ and $m_{\tilde{\chi}_1^0}$ even outside the kinematic region that the search was initially designed to cover.

4 Exclusion limits for purely right-handed up-squark mixing

In order to illustrate the effects of flavour mixing in the up-squark sector, we consider a simplified model consisting of a bino-like LSP and a purely right-handed top-like squark \tilde{t}_1 that is an admixture of \tilde{t}_R and \tilde{c}_R flavour eigenstates. Since $\tilde{t}_R - \tilde{c}_R$ mixing is induced by flavour non-diagonal entries in the squark mass-squared matrix $M_{\tilde{u}}^2$, it is convenient to use the mass insertion method [45] to express flavour constraints in terms of the dimensionless quantity

$$\delta_{RR}^u = \frac{(M_{\tilde{u}}^2)_{23}}{(M_{\tilde{u}})_{22}(M_{\tilde{u}})_{33}}. \quad (4.1)$$

In contrast to quantities like δ_{LL}^u or δ_{RL}^u where mixing with \tilde{t}_L is considered, purely right-handed scenarios do not require a light bottom squark, and are hence not subject to strong constraints from direct sbottom searches [26, 46–48]. Quark flavour constraints are also avoided if only δ_{RR}^u insertions are considered. We note that although the mass insertion parameter δ_{LR}^u does not require a light sbottom and is poorly constrained by flavour physics, its effect on the stop decay width is suppressed relative to δ_{RR}^u by a factor of 16 due to hypercharges. Using the mass insertion parameter (4.1) as a template thus allows one to illustrate the maximal effects of flavour violation in stop decays. Choosing

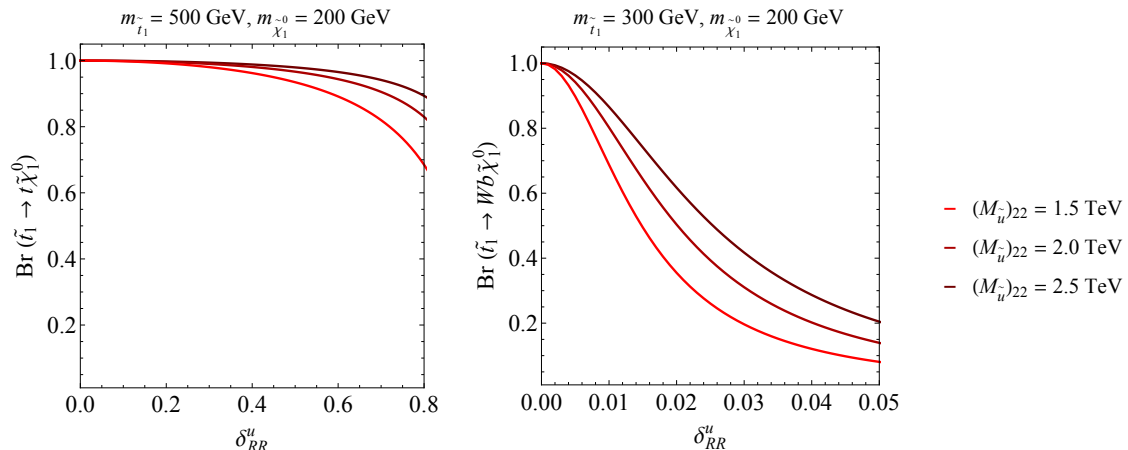


Figure 8. The branching ratios $\text{Br}(\tilde{t}_1 \rightarrow t\tilde{\chi}_1^0)$ (left panel) and $\text{Br}(\tilde{t}_1 \rightarrow Wb\tilde{\chi}_1^0)$ (right panel) as a function of the mass insertion parameter δ_{RR}^u . The lightest stop mass and the LSP mass have been fixed to $m_{\tilde{t}_1} = 500$ GeV and $m_{\tilde{\chi}_1^0} = 200$ GeV ($m_{\tilde{t}_1} = 300$ GeV and $m_{\tilde{\chi}_1^0} = 200$ GeV) to obtain the left (right) plot. The different curves in the panels correspond to different choices of $(M_{\tilde{u}})_{22}$ as indicated by the legend on the right-hand side in the figure.

other possibilities would generically lead to stronger exclusions, once additional direct and/or indirect constraints are included.

In Figure 8, we show the dependence of $\text{Br}(\tilde{t}_1 \rightarrow t\tilde{\chi}_1^0)$ and $\text{Br}(\tilde{t}_1 \rightarrow Wb\tilde{\chi}_1^0)$ on δ_{RR}^u for three different benchmark values of $(M_{\tilde{u}})_{22}$. The left panel corresponds to $m_{\tilde{t}_1} = 500$ GeV and $m_{\tilde{\chi}_1^0} = 200$ GeV, i.e. a parameter point that lies in the heart of the kinematic region R1. Similarly, the curves in the right panel are based on the point $m_{\tilde{t}_1} = 300$ GeV and $m_{\tilde{\chi}_1^0} = 200$ GeV, which is located in the kinematic region R2. Note that even though we parameterise our results in terms of (4.1), we perform an exact diagonalisation in our numerical analysis. One observes that to reduce $\text{Br}(\tilde{t}_1 \rightarrow t\tilde{\chi}_1^0) = 1 - \text{Br}(\tilde{t}_1 \rightarrow c\tilde{\chi}_1^0)$ from 100% to 90% requires large mass insertions $\delta_{RR}^u \in [0.6, 0.8]$, while values of $\delta_{RR}^u \simeq 0.02$ are sufficient to suppress $\text{Br}(\tilde{t}_1 \rightarrow Wb\tilde{\chi}_1^0) = 1 - \text{Br}(\tilde{t}_1 \rightarrow c\tilde{\chi}_1^0)$ by approximately 50%. The strong δ_{RR}^u -dependence of $\text{Br}(\tilde{t}_1 \rightarrow Wb\tilde{\chi}_1^0)$ is a consequence of the fact that $\tilde{t}_1 \rightarrow Wb\tilde{\chi}_1^0$ is a three-body decay, whereas $\tilde{t}_1 \rightarrow c\tilde{\chi}_1^0$ is a two-body process. In the case of $\tilde{t}_1 \rightarrow t\tilde{\chi}_1^0$, the flavour-conserving decay mode is not phase-space suppressed and as a result a larger $\tilde{t}_R - \tilde{c}_R$ mixing angle is needed to obtain appreciable values of $\text{Br}(\tilde{t}_1 \rightarrow c\tilde{\chi}_1^0)$. In the kinematic region R3, $\tilde{t}_1 \rightarrow c\tilde{\chi}_1^0$ is the dominant decay mode unless δ_{RR}^u is below 10^{-3} , in which case the four-body mode $\tilde{t}_1 \rightarrow bff'\tilde{\chi}_1^0$ becomes the main channel. In the following, we will not consider such small $\tilde{t}_R - \tilde{c}_R$ mixing angles and hence will employ $\text{Br}(\tilde{t}_1 \rightarrow c\tilde{\chi}_1^0) = 100\%$ in the whole region R3.

In the two panels of Figure 9, we show the results of the combined search strategies of Sections 2 and 3 when applied to two representative scenarios of $\tilde{t}_R - \tilde{c}_R$ mixing. The left panel depicts the case of large mixing $\delta_{RR}^u = 0.7$, while the right panel illustrates the case of small mixing $\delta_{RR}^u = 0.02$. In both plots, we have fixed $(M_{\tilde{u}})_{22} = 1.5$ TeV and the red contours correspond to the regions in the $m_{\tilde{t}_1} - m_{\tilde{\chi}_1^0}$ plane that are excluded at 95% CL. To guide the eye, the 95% CL exclusion limits obtained in [19] and [31] have been overlaid as

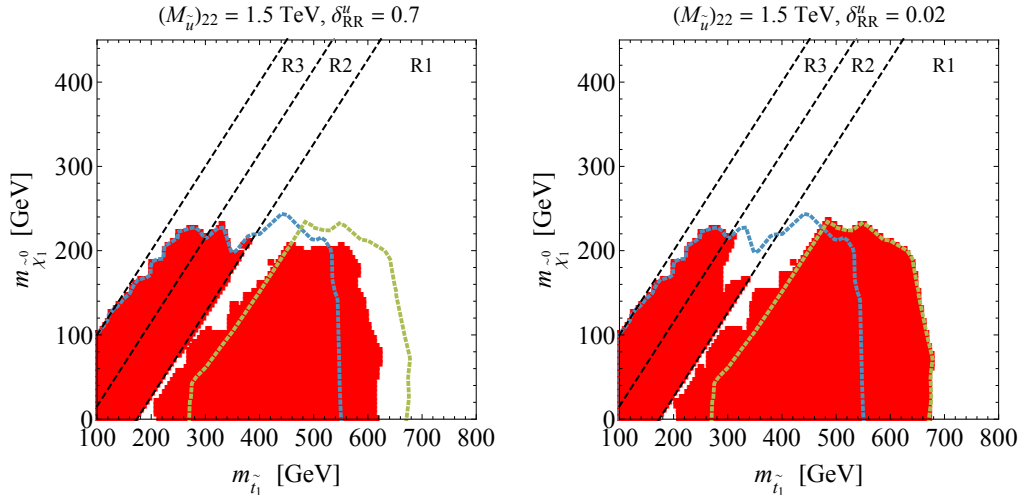


Figure 9. 95% CL exclusion regions in the $m_{\tilde{t}_1} - m_{\tilde{\chi}_1^0}$ plane for two representative $\tilde{t}_R - \tilde{c}_R$ mixing scenarios. The left (right) panel employs the parameters $(M_{\tilde{u}})_{22} = 1.5$ TeV and $\delta_{RR}^u = 0.7$ ($(M_{\tilde{u}})_{22} = 1.5$ TeV and $\delta_{RR}^u = 0.02$). For comparison also the exclusion limits at 95% CL following from the 1 lepton + 4 jets + 1 b -tag + $E_{T,\text{miss}}$ search [19] (green dotted curves) and the 2 c -tags + $E_{T,\text{miss}}$ search [31] (blue dotted curves) are overlaid.

green and blue dotted curves. Focusing our attention on the kinematic region R1, we see that for the choice $\delta_{RR}^u = 0.7$ the limits on $m_{\tilde{t}_1}$ are about 50 GeV weaker than the bounds obtained in [19], which assumes no stop-scharm mixing. On the other hand, for $\delta_{RR}^u = 0.02$ our exclusion coincides with the limit of the 1 lepton + 4 jets + 1 b -tag + $E_{T,\text{miss}}$ search. These features are expected because in the first case one has $\text{Br}(\tilde{t}_1 \rightarrow t\tilde{\chi}_1^0) \in [70, 80]\%$ in the parameter space of interest, while $\text{Br}(\tilde{t}_1 \rightarrow t\tilde{\chi}_1^0) \simeq 100\%$ in the second case. In the kinematic region R2, one observes instead that for large $\tilde{t}_R - \tilde{c}_R$ mixing our bound resembles that of the analysis [31], while for small mixing the region in the $m_{\tilde{t}_1} - m_{\tilde{\chi}_1^0}$ plane around $m_{\tilde{t}_1} = 300$ GeV and $m_{\tilde{\chi}_1^0} = 200$ GeV remains allowed. These properties can be understood by realising that in the first case the lightest stop decays to almost 100% via $\tilde{t}_1 \rightarrow c\tilde{\chi}_1^0$, while in the second case the decay mode $\tilde{t}_1 \rightarrow Wb\tilde{\chi}_1^0$ is dominant, in particular for values of the stop and LSP mass close to the kinematic boundary $m_{\tilde{t}_1} - m_{\tilde{\chi}_1^0} = m_t$. One furthermore notices, that in region R3 our exclusions match the 95% CL bound from the $\tilde{c}_1 \rightarrow c\tilde{\chi}_1^0$ analysis [31], since both our choices of δ_{RR}^u lead to $\text{Br}(\tilde{t}_1 \rightarrow c\tilde{\chi}_1^0) = 100\%$. The two scenarios of $\tilde{t}_R - \tilde{c}_R$ mixing that we have considered nicely illustrate our general finding that by combining various $E_{T,\text{miss}}$ search strategies, large regions in the $m_{\tilde{t}_1} - m_{\tilde{\chi}_1^0}$ plane can be excluded for arbitrary mass insertion parameters δ_{RR}^u .

Notice that quark flavour observables leave the mass insertion parameter δ_{RR}^u essentially unconstrained. Although $\tilde{t}_R - \tilde{c}_R$ mixing will induce flavour-changing top-quark decays like $t \rightarrow cZ$ and $t \rightarrow ch$ at the one-loop level, the existing LHC Run I constraints on the relevant processes [49] are too loose to lead to any restriction. The mass insertion parameter δ_{RR}^u also modifies B -meson decays via chargino loops. However, the wino couples only to left-handed squarks and the Higgsino coupling to right-handed squarks is proportional to the corresponding Yukawa coupling, which is small in the case of the

charm squark. As a result, corrections associated to the δ_{RR}^u mass insertion are strongly suppressed in processes like $B_s \rightarrow \mu^+ \mu^-$ and $B \rightarrow X_s \gamma$, making the constraints from stop searches derived above the only relevant restrictions on scenarios with purely right-handed stop-scharm mixing.

5 Conclusions and outlook

In this article, we have shown that allowing for non-minimal flavour violation in the up-squark sector of the MSSM can weaken the direct LHC bounds on the mass $m_{\tilde{t}_1}$ of the lightest stop. While large effects were found previously [27–29], we have demonstrated that a detailed numerical analysis which includes the recent ATLAS search for $\tilde{c}_1 \rightarrow c\tilde{\chi}_1^0$ limits the possible impact of $\tilde{t}_1 \rightarrow c\tilde{\chi}_1^0$ on $\tilde{t}_1 \rightarrow c\tilde{\chi}_1^0$ and $\tilde{t}_1 \rightarrow Wb\tilde{\chi}_1^0$. The general idea is that although an enhanced $\tilde{t}_1 \rightarrow c\tilde{\chi}_1^0$ decay rate decreases the branching ratios of $\tilde{t}_1 \rightarrow t\tilde{\chi}_1^0$ and $\tilde{t}_1 \rightarrow Wb\tilde{\chi}_1^0$, the direct $\tilde{c}_1 \rightarrow c\tilde{\chi}_1^0$ bounds become progressively more relevant, and as a result stop and scharm searches cannot be fully decoupled in the presence of up-squark mixing. By combining the different decay channels, we demonstrated that there are large regions in the $m_{\tilde{t}_1} - m_{\tilde{\chi}_1^0}$ plane which are disfavoured by LHC Run I searches, independently of the amount of stop-scharm mixing. In particular, we find a lower limit of $m_{\tilde{t}_1} > 530$ GeV at 95% CL for LSP masses $m_{\tilde{\chi}_1^0} \lesssim 100$ GeV. This finding agrees with [30], generalising it to the case of a neutralino with non-zero mass. Stringent exclusion limits can also be derived for all other considered decay scenarios. We have illustrated this point by studying MSSM scenarios with a bino-like LSP and non-zero $\tilde{t}_R - \tilde{c}_R$ mixing. The two representative cases of the mass insertion parameter δ_{RR}^u that we have considered are left unconstrained by quark flavour observables, but by combining various direct $E_{T,\text{miss}}$ searches, stringent exclusions in the $m_{\tilde{t}_1} - m_{\tilde{\chi}_1^0}$ plane can be derived.

In LHC Run II and beyond, the ATLAS and CMS collaborations are expected to provide new results on stop searches with a significantly improved reach in the $m_{\tilde{t}_1} - m_{\tilde{\chi}_1^0}$ plane. Improvements in the sensitivity to stops will not only be due to the increase in the centre-of-mass energy, but is also likely to arise from new analysis strategies or technical developments. For instance, ATLAS has recently installed [50] a new subdetector called Insertable B-Layer or IBL [51]. This new inner pixel layer should allow to improve the c -tagging capabilities of ATLAS and thus pave the way to look for processes like $\tilde{c}_1 \rightarrow c\tilde{\chi}_1^0$ and $\tilde{t}_1 \rightarrow c\tilde{\chi}_1^0$ in a more efficient fashion. The complementarity and synergy between the different stop decay channels that exists in the presence of flavour mixing is therefore expected to become phenomenologically even more relevant at later phases of the LHC physics programme.

Acknowledgments

We thank William Kalderon for useful discussions concerning the ATLAS search for scalar charm quarks [31]. The work of AC was supported by a Marie Curie Intra-European Fellowship of the European Community’s 7th Framework Programme (contract number

PIEF-GA-2012-326948) and by an Ambizione Grant of the Swiss National Science Foundation. UH acknowledges the hospitality and support of the CERN theory division. He also would like to thank the KITP in Santa Barbara for hospitality and acknowledges that this research was supported in part by the National Science Foundation under Grant No. NSF PHY11-25915. LCT is supported by the Swiss National Science Foundation.

A Event generation

Our event generation has been performed at leading order with `MadGraph5_aMCNLO` [52] starting from a customised version of the implementation of coloured scalar pair production presented in [53] and utilises `NNPDF2.3` parton distribution functions [54]. The simulated parton-level events were showered with `PYTHIA 6` [55] and analysed with the publicly available code `CheckMATE` [56], which relies on `DELPHES 3` [57] as a fast detector simulation. In order to be able to distinguish charm-quark jets from both bottom-quark and light-flavoured jets, we have implemented the `JetFitterCharm` algorithm described in [36] into `DELPHES 3`. In all our analyses jets were clustered with `FastJet` [58] with the anti- k_t algorithm [59] as the standard jet finder.

The efficiency maps presented in Figures 2 and 6 have been obtained by simulating 138 different signal points that fall into the kinematic regions R1 and R2. The actual mapping in the $m_{\tilde{t}_1} - m_{\tilde{\chi}_1^0}$ plane can be found in [60, 61]. For each signal point and all relevant final states, 10^5 partonic events have been generated, showered and passed through the fast detector simulation and an analysis containing the selection requirements corresponding to the individual searches described in Sections 2 and 3. The efficiency maps are then obtained by considering the SR that provides the best exclusion limit for a given point in the $m_{\tilde{t}_1} - m_{\tilde{\chi}_1^0}$ plane.

References

- [1] S. Dimopoulos and G. F. Giudice, *Naturalness constraints in supersymmetric theories with nonuniversal soft terms*, *Phys. Lett.* **B357** (1995) 573–578, [[hep-ph/9507282](#)].
- [2] A. Pomarol and D. Tommasini, *Horizontal symmetries for the supersymmetric flavor problem*, *Nucl. Phys.* **B466** (1996) 3–24, [[hep-ph/9507462](#)].
- [3] A. G. Cohen, D. B. Kaplan, and A. E. Nelson, *The More minimal supersymmetric standard model*, *Phys. Lett.* **B388** (1996) 588–598, [[hep-ph/9607394](#)].
- [4] R. Kitano and Y. Nomura, *Supersymmetry, naturalness, and signatures at the LHC*, *Phys. Rev.* **D73** (2006) 095004, [[hep-ph/0602096](#)].
- [5] C. Brust, A. Katz, S. Lawrence, and R. Sundrum, *SUSY, the Third Generation and the LHC*, *JHEP* **03** (2012) 103, [[1110.6670](#)].
- [6] M. Papucci, J. T. Ruderman, and A. Weiler, *Natural SUSY Endures*, *JHEP* **09** (2012) 035, [[1110.6926](#)].
- [7] P. Batra, A. Delgado, D. E. Kaplan, and T. M. P. Tait, *The Higgs mass bound in gauge extensions of the minimal supersymmetric standard model*, *JHEP* **02** (2004) 043, [[hep-ph/0309149](#)].

- [8] L. J. Hall, D. Pinner, and J. T. Ruderman, *A Natural SUSY Higgs Near 126 GeV*, *JHEP* **04** (2012) 131, [[1112.2703](#)].
- [9] S. P. Martin, *A Supersymmetry primer*, [hep-ph/9709356](#).
- [10] C. Boehm, A. Djouadi, and M. Drees, *Light scalar top quarks and supersymmetric dark matter*, *Phys. Rev.* **D62** (2000) 035012, [[hep-ph/9911496](#)].
- [11] J. R. Ellis, K. A. Olive, and Y. Santoso, *Calculations of neutralino stop coannihilation in the CMSSM*, *Astropart. Phys.* **18** (2003) 395–432, [[hep-ph/0112113](#)].
- [12] M. Carena, M. Quiros, and C. E. M. Wagner, *Opening the window for electroweak baryogenesis*, *Phys. Lett.* **B380** (1996) 81–91, [[hep-ph/9603420](#)].
- [13] J. R. Espinosa, *Dominant two loop corrections to the MSSM finite temperature effective potential*, *Nucl. Phys.* **B475** (1996) 273–292, [[hep-ph/9604320](#)].
- [14] D. Delepine, J. M. Gerard, R. Gonzalez Felipe, and J. Weyers, *A Light stop and electroweak baryogenesis*, *Phys. Lett.* **B386** (1996) 183–188, [[hep-ph/9604440](#)].
- [15] **ATLAS**, *Summary plots from the ATLAS Supersymmetry physics group*.
- [16] **CMS**, *Summary of comparison plots in simplified models spectra for the 8 TeV dataset*.
- [17] **ATLAS**, G. Aad et al., *Search for direct top-squark pair production in final states with two leptons in pp collisions at $\sqrt{s} = 8$ TeV with the ATLAS detector*, *JHEP* **06** (2014) 124, [[1403.4853](#)].
- [18] **ATLAS**, G. Aad et al., *Search for direct pair production of the top squark in all-hadronic final states in proton-proton collisions at $\sqrt{s} = 8$ TeV with the ATLAS detector*, *JHEP* **09** (2014) 015, [[1406.1122](#)].
- [19] **ATLAS**, G. Aad et al., *Search for top squark pair production in final states with one isolated lepton, jets, and missing transverse momentum in $\sqrt{s} = 8$ TeV pp collisions with the ATLAS detector*, *JHEP* **11** (2014) 118, [[1407.0583](#)].
- [20] **CMS**, S. Chatrchyan et al., *Search for top-squark pair production in the single-lepton final state in pp collisions at $\sqrt{s} = 8$ TeV*, *Eur. Phys. J.* **C73** (2013), no. 12 2677, [[1308.1586](#)].
- [21] **CMS**, *Search for top squarks in multijet events with large missing momentum in proton-proton collisions at 8 TeV*.
- [22] **CMS**, *Exclusion limits on gluino and top-squark pair production in natural SUSY scenarios with inclusive razor and exclusive single-lepton searches at 8 TeV*.
- [23] **ATLAS**, *Search for top squarks in final states with one isolated lepton, jets, and missing transverse momentum in $\sqrt{s} = 13$ TeV pp collisions of ATLAS data*.
- [24] **ATLAS**, *Search for direct top squark pair production in final states with two leptons in $\sqrt{s} = 13$ TeV pp collisions using 3.2 fb^{-1} of ATLAS data*.
- [25] **CMS**, *Search for direct top squark pair production in the single lepton final state at $\sqrt{s} = 13$ TeV*.
- [26] **CMS**, *Further SUSY Simplified Model interpretations for Moriond 2016*.
- [27] A. Bartl, H. Eberl, E. Ginina, B. Herrmann, K. Hidaka, et al., *Flavor violating bosonic squark decays at LHC*, *Int. J. Mod. Phys.* **A29** (2014), no. 07 1450035, [[1212.4688](#)].
- [28] M. Blanke, G. F. Giudice, P. Paradisi, G. Perez, and J. Zupan, *Flavoured Naturalness*, *JHEP* **06** (2013) 022, [[1302.7232](#)].

- [29] P. Agrawal and C. Frugiuele, *Mixing stops at the LHC*, *JHEP* **01** (2014) 115, [[1304.3068](#)].
- [30] M. Blanke, B. Fuks, I. Galon, and G. Perez, *Gluino Meets Flavored Naturalness*, [1512.03813](#).
- [31] **ATLAS**, G. Aad et al., *Search for Scalar Charm Quark Pair Production in pp Collisions at $\sqrt{s} = 8$ TeV with the ATLAS Detector*, *Phys. Rev. Lett.* **114** (2015), no. 16 161801, [[1501.01325](#)].
- [32] R. Gröber, M. Mühlleitner, E. Popenza, and A. Wlotzka, *Light stop decays into $Wb\tilde{\chi}_1^0$ near the kinematic threshold*, *Phys. Lett.* **B747** (2015) 144–151, [[1502.05935](#)].
- [33] **ATLAS**, G. Aad et al., *Search for pair-produced third-generation squarks decaying via charm quarks or in compressed supersymmetric scenarios in pp collisions at $\sqrt{s} = 8$ TeV with the ATLAS detector*, *Phys. Rev.* **D90** (2014), no. 5 052008, [[1407.0608](#)].
- [34] R. Gröber, M. M. Mühlleitner, E. Popenza, and A. Wlotzka, *Light Stop Decays: Implications for LHC Searches*, *Eur. Phys. J.* **C75** (2015) 420, [[1408.4662](#)].
- [35] G. Polesello and D. R. Tovey, *Supersymmetric particle mass measurement with the boost-corrected contranverse mass*, *JHEP* **03** (2010) 030, [[0910.0174](#)].
- [36] **ATLAS**, *Performance and Calibration of the JetFitterCharm Algorithm for c-Jet Identification*.
- [37] **ATLAS**, *Calibrating the b-Tag Efficiency and Mistag Rate in 35 pb^{-1} of Data with the ATLAS Detector*.
- [38] **ATLAS**, *Commissioning of the ATLAS high-performance b-tagging algorithms in the 7 TeV collision data*.
- [39] H.-C. Cheng and Z. Han, *Minimal Kinematic Constraints and m_{T2}* , *JHEP* **12** (2008) 063, [[0810.5178](#)].
- [40] A. J. Barr, B. Gripaios, and C. G. Lester, *Transverse masses and kinematic constraints: from the boundary to the crease*, *JHEP* **11** (2009) 096, [[0908.3779](#)].
- [41] P. Konar, K. Kong, K. T. Matchev, and M. Park, *Dark Matter Particle Spectroscopy at the LHC: Generalizing m_{T2} to Asymmetric Event Topologies*, *JHEP* **04** (2010) 086, [[0911.4126](#)].
- [42] Y. Bai, H.-C. Cheng, J. Gallicchio, and J. Gu, *Stop the Top Background of the Stop Search*, *JHEP* **07** (2012) 110, [[1203.4813](#)].
- [43] C. G. Lester and D. J. Summers, *Measuring masses of semiinvisibly decaying particles pair produced at hadron colliders*, *Phys. Lett.* **B463** (1999) 99–103, [[hep-ph/9906349](#)].
- [44] A. Barr, C. Lester, and P. Stephens, *m_{T2} : the truth behind the glamour*, *J. Phys.* **G29** (2003) 2343–2363, [[hep-ph/0304226](#)].
- [45] F. Gabbiani, E. Gabrielli, A. Masiero, and L. Silvestrini, *A Complete analysis of FCNC and CP constraints in general SUSY extensions of the standard model*, *Nucl. Phys.* **B477** (1996) 321–352, [[hep-ph/9604387](#)].
- [46] **ATLAS**, G. Aad et al., *Search for direct third-generation squark pair production in final states with missing transverse momentum and two b-jets in $\sqrt{s} = 8$ TeV pp collisions with the ATLAS detector*, *JHEP* **10** (2013) 189, [[1308.2631](#)].
- [47] **CMS**, *Search for direct production of bottom squark pairs*.
- [48] **ATLAS**, *Search for Bottom Squark Pair Production with the ATLAS Detector in proton-proton Collisions at $\sqrt{s} = 13$ TeV*.

- [49] A. Loginov, *ATLAS + CMS top production and properties: run 1 legacy*.
- [50] A. E. Phoboo and C. O’Luanaigh, *A new subdetector for ATLAS*.
- [51] M. Capeans, G. Darbo, K. Einsweiler, M. Elsing, T. Flick, et al., *ATLAS Insertable B-Layer Technical Design Report*.
- [52] J. Alwall, R. Frederix, S. Frixione, V. Hirschi, F. Maltoni, et al., *The automated computation of tree-level and next-to-leading order differential cross sections, and their matching to parton shower simulations*, *JHEP* **07** (2014) 079, [[1405.0301](#)].
- [53] C. Degrande, B. Fuks, V. Hirschi, J. Proudom, and H.-S. Shao, *Automated next-to-leading order predictions for new physics at the LHC: the case of colored scalar pair production*, *Phys. Rev.* **D91** (2015), no. 9 094005, [[1412.5589](#)].
- [54] R. D. Ball et al., *Parton distributions with LHC data*, *Nucl. Phys.* **B867** (2013) 244–289, [[1207.1303](#)].
- [55] T. Sjostrand, S. Mrenna, and P. Z. Skands, *PYTHIA 6.4 Physics and Manual*, *JHEP* **05** (2006) 026, [[hep-ph/0603175](#)].
- [56] M. Drees, H. Dreiner, D. Schmeier, J. Tattersall, and J. S. Kim, *CheckMATE: Confronting your Favourite New Physics Model with LHC Data*, *Comput. Phys. Commun.* **187** (2014) 227–265, [[1312.2591](#)].
- [57] **DELPHES 3**, J. de Favereau, C. Delaere, P. Demin, A. Giammanco, V. Lematre, et al., *DELPHES 3, A modular framework for fast simulation of a generic collider experiment*, *JHEP* **02** (2014) 057, [[1307.6346](#)].
- [58] M. Cacciari, G. P. Salam, and G. Soyez, *FastJet User Manual*, *Eur. Phys. J.* **C72** (2012) 1896, [[1111.6097](#)].
- [59] M. Cacciari, G. P. Salam, and G. Soyez, *The anti- k_t jet clustering algorithm*, *JHEP* **04** (2008) 063, [[0802.1189](#)].
- [60] **HepData**, *AAD 2014 — Search for top squark pair production in final states with one isolated lepton, jets, and missing transverse momentum in $\sqrt{s} = 8$ TeV pp collisions with the ATLAS detector*.
- [61] **HepData**, *AAD 2015 — Search for Scalar Charm Quark Pair Production in pp Collisions at $\sqrt{s} = 8$ TeV with the ATLAS Detector*.